

Synchronization of two self-excited double pendula

Piotr Koluda¹, Przemyslaw Perlikowski^{1,a}, Krzysztof Czołczynski¹, and Tomasz Kapitaniak¹

Division of Dynamics, Faculty of Mechanical Engineering, Lodz University of Technology, 90-924 Lodz, Stefanowskiego 1/15, Poland

Abstract. We consider the synchronization of two self-excited double pendula. We show that such pendula hanging on the same beam can have four different synchronous configurations. Our approximate analytical analysis allows us to derive the synchronization conditions and explain the observed types of synchronization. We consider an energy balance in the system and describe how the energy is transferred between the pendula via the oscillating beam, allowing thus the pendula synchronization. Changes and stability ranges of the obtained solutions with increasing and decreasing masses of the pendula are shown using path-following.

1 Introduction

Synchronization is commonly observed to occur among oscillators [1,2,3,4,5]. It is a process where two or more systems interact with one another and come to oscillate together. Groups of oscillators are observed to synchronize in a diverse variety of systems, despite inevitable differences between oscillators. The history of synchronization goes back to the 17th century. In 1673 the Dutch scientist Ch. Huygens observed weak synchronization of two pendulum clocks [6]. Recently, the phenomenon of synchronization of clocks hanging on a common movable beam [7] has been the subject of research conducted by numerous authors [6,8,9,10,11,12,13,14,15,16,17,18]. These studies explain the phenomenon of synchronization of a number of single pendula.

In our work we consider an interaction between two double pendula. One of the first investigations on dynamics of the double pendulum can be found in the paper by Rott [19], where an analytical investigation of the Hamiltonian system for different ratios between natural frequencies of pendula is presented. The next results obtained by Miles [20] show dynamics of the double pendulum under parametric excitation around the $2 : 1$ resonance. A mode interaction in the double pendulum, including a detailed bifurcation analysis near two multiple bifurcation points and a transition to quasi-periodic motion and chaos around the $2 : 1$ parametric resonance, is presented in [21,22,23]. Similarly as for $2 : 1$, the $1 : 1$ resonance leads to dynamics including multiple bifurcation points, symmetry breaking and cascades of period doubling bifurcations [23]. Double pendula can be also considered as an example of many physical

^a e-mail: przemyslaw.perlikowski@p.lodz.pl

systems commonly met in engineering, e.g., a model of bridge-pedestrian interactions [24], golf or hockey swing interactions with arms [25], human body [26] or trunk [27] models.

In this paper we consider the synchronization of two self-excited double pendula. The oscillations of each double pendulum are self-excited by the van der Pol type of damping associated with the upper parts (upper pendula) of each double pendulum. We show that two such double pendula hanging on the same beam can synchronize both in phase and in anti-phase. We give an evidence that the observed synchronous states are robust as they exist for a wide range of system parameters and are preserved for the parameter mismatch. The performed approximate analytical analysis allows us to derive the synchronization conditions and explain the observed types of synchronization. The energy balance in the system allows us to show how the energy is transferred between the pendula via the oscillating beam.

This paper is organized as follows: Section 2 describes the considered model of the coupled double pendula, in Section 3 we derive an energy balance of the synchronized pendula, whereas Section 4 presents the results of our numerical simulations and describes the observed synchronization states and their ranges of stability. Finally, we summarize our results in Section 5.

2 Model

The analyzed system is shown in Fig. 1. It consists of a rigid beam and two double pendula suspended on it. The beam of the mass M can move along the horizontal direction, its movement is described by the coordinate x_b . The beam is connected to a linear spring and a linear damper, k_x and c_x .

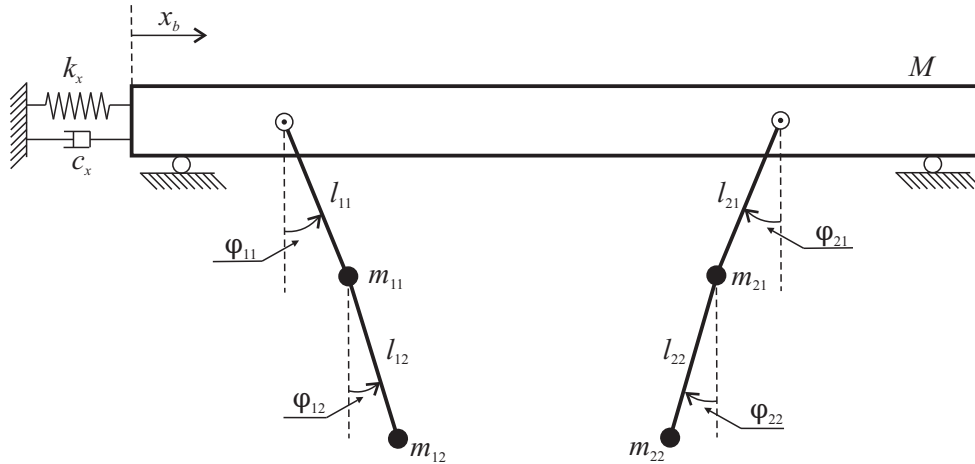


Fig. 1. Model of the system - two double pendula are mounted to the beam which can move horizontally. Each double pendulum consists of an upper pendulum of the length l_{i1} and the mass m_{i1} and a lower pendulum of the length l_{i2} and the mass m_{i2} ($i = 1, 2$). The upper pendula are self-excited.

Each double pendulum consists of two light beams of the length l_{i1} and the masses m_{i1} (i -th upper pendulum) and the length l_{i2} and m_{i2} (i -th lower pendulum), where $i = 1, 2$, mounted at its ends. We consider double pendula with the same lengths $l_{11} = l_{21} = l_{12} = l_{22} = l$ but different masses m_{i1} and m_{i2} (to maintain generality in

the derivation of equations, we use indexes for lengths of the pendula). The motion of each double pendulum is described by the angles φ_{i1} (upper pendulum) and φ_{i2} (lower pendulum). The upper pendula are self-excited by the van der Pol type of damping (not shown in Fig. 1) given by the momentum (torque) $c_{vdp}\dot{\varphi}_{1i}(1 - \mu\varphi_{1i}^2)$, where c_{vdp} and μ are constant. Van der Pol damping results in the generation of a stable limit cycle [1]. The lower pendula are damped with a viscous damper with the coefficient c_{i2} . The equations of motion of the considered system are as follows:

$$\begin{aligned} & (M + \sum_{i=1}^2 \sum_{j=1}^2 m_{ij})\ddot{x}_b + \sum_{i=1}^2 (m_{i1} + m_{i2})l_{i1}(\ddot{\varphi}_{i1} \cos \varphi_{i1} - \dot{\varphi}_{i1}^2 \sin \varphi_{i1}) + \\ & \sum_{i=1}^2 m_{i2}l_{i2}(\ddot{\varphi}_{i2} \cos \varphi_{i2} - \dot{\varphi}_{i2}^2 \sin \varphi_{i2}) + k_x x_b + c_x \dot{x}_b = 0 \\ & (m_{i1} + m_{i2})l_{i1}\ddot{x}_b \cos \varphi_{i1} + (m_{i1} + m_{i2})l_{i1}^2\ddot{\varphi}_{i1} + m_{i2}l_{i1}l_{i2}\ddot{\varphi}_{i2} \cos(\varphi_{i1} - \varphi_{i2}) + \\ & m_{i2}l_{i1}l_{i2}\dot{\varphi}_{i2}^2 \sin(\varphi_{i1} - \varphi_{i2}) + (m_{i1} + m_{i2})l_{i1}g \sin(\varphi_{i1}) + c_{vdp}(1 - \mu\varphi_{i1}^2)\dot{\varphi}_{i1} + c_{i2}(\dot{\varphi}_{i2} - \dot{\varphi}_{i1}) = 0 \\ & m_{i2}l_{i2}\ddot{x}_b \cos \varphi_{i2} + m_{i2}l_{i1}l_{i2}\ddot{\varphi}_{i1} \cos(\varphi_{i1} - \varphi_{i2}) + m_{i2}l_{i2}^2\ddot{\varphi}_{i2} \\ & - m_{i2}l_{i1}l_{i2}\dot{\varphi}_{i1}^2 \sin(\varphi_{i1} - \varphi_{i2}) + m_{i2}l_{i2}g \sin(\varphi_{i2}) - c_{i2}(\dot{\varphi}_{i2} - \dot{\varphi}_{i1}) = 0. \end{aligned} \quad (1)$$

Introducing the dimensionless time $\tau = \omega t$, where $\omega^2 = \frac{g}{l_{i1}}$ is the natural frequency of the upper pendula, we can rewrite Eq. (1) in the dimensionless form as:

$$\ddot{y}_b + \sum_{i=1}^2 \mathbf{A}_{i1}(\ddot{\psi}_{i1} \cos \psi_{i1} - \dot{\psi}_{i1}^2 \sin \psi_{i1}) + \sum_{i=1}^2 \mathbf{A}_{i2}(\ddot{\psi}_{i2} \cos \psi_{i2} - \dot{\psi}_{i2}^2 \sin \psi_{i2}) + \quad (2)$$

$$+ \mathbf{K}y_b + \mathbf{C}\dot{y}_b = 0$$

$$\delta_{i1}\ddot{y}_b \cos \psi_{i1} + \mathbf{L}_{i1}\ddot{\psi}_{i1} + \mathbf{L}_{i3}\ddot{\psi}_{i2} \cos(\psi_{i1} - \psi_{i2}) = \quad (3)$$

$$- \mathbf{L}_{i3}\dot{\psi}_{i2}^2 \sin(\psi_{i1} - \psi_{i2}) - \mathbf{G}_{i1} \sin(\psi_{i1}) - \mathbf{C}_{vdp}(1 - \mu\psi_{i1}^2)\dot{\psi}_{i1} - \mathbf{C}_{i2}(\dot{\psi}_{i2} - \dot{\psi}_{i1})$$

$$\delta_{i2}\ddot{y}_b \cos \psi_{i2} + \mathbf{L}_{i3}\ddot{\psi}_{i1} \cos(\psi_{i1} - \psi_{i2}) + \mathbf{L}_{i2}\ddot{\psi}_{i2} = \quad (4)$$

$$\mathbf{L}_{i3}\dot{\psi}_{i1}^2 \sin(\psi_{i1} - \psi_{i2}) - \mathbf{G}_{i2} \sin(\psi_{i2}) + \mathbf{C}_{i2}(\dot{\psi}_{i2} - \dot{\psi}_{i1})$$

where $\mathbf{A}_{i1} = \frac{(m_{i1}+m_{i2})l_{i1}}{Ml_b}$, $\mathbf{A}_{i2} = \frac{m_{i2}l_{i2}}{Ml_b}$, $\mathbf{K} = \frac{k_x}{M\omega^2}$, $\mathbf{C} = \frac{c_x}{M\omega}$, $\delta_{i1} = \frac{(m_{i1}+m_{i2})l_{i1}}{Ml_{i2}}$, $\delta_{i2} = \frac{m_{i2}l_{i2}}{Ml_{i2}}$, $\mathbf{L}_{i1} = \frac{(m_{i1}+m_{i2})l_{i1}^2}{l_{i2}l_bM}$, $\mathbf{L}_{i2} = \frac{m_{i2}l_{i2}^2}{l_{i2}l_bM}$, $\mathbf{L}_{i3} = \frac{m_{i2}l_{i2}l_{i1}}{l_bMl_{i2}}$, $\mathbf{G}_{i1} = \frac{(m_{i1}+m_{i2})l_{i1}g}{l_{i2}\omega^2l_bM}$, $\mathbf{G}_{i2} = \frac{m_{i2}l_{i2}g}{l_{i2}\omega^2l_bM}$, $\mathbf{C}_{vdp} = \frac{c_{vdp}}{\omega l_b M l_{i2}}$, $\mathbf{C}_{i2} = \frac{c_{i2}}{l_{i2}\omega l_b M}$.

3 Analytical conditions for synchronization

3.1 Force with which the pendula act on the beam

In this section we derive an approximate analytical condition for the pendulum synchronization in the considered system. Assuming that the double pendula are identical and perform periodic oscillations with the frequency ω_0 and low amplitudes, one can describe displacements, velocities and accelerations of the upper and lower pendula in the following way:

$$\psi_{ij} = \Phi_{ij} \sin(\omega_0\tau + \beta_{ij}), \quad (5)$$

$$\dot{\psi}_{ij} = \omega_0\Phi_{ij} \cos(\omega_0\tau + \beta_{ij}), \quad (6)$$

$$\ddot{\psi}_{ij} = -\omega_0^2\Phi_{ij} \sin(\omega_0\tau + \beta_{ij}), \quad (7)$$

where β_{ij} ($i, j = 1, 2$) are phase differences between the pendula.

Equation (2) allows an estimation of the resultant force with which the pendula act on the beam:

$$F = - \sum_{i=1}^2 \mathbf{A}_{i1} (\ddot{\psi}_{i1} \cos \psi_{i1} - \dot{\psi}_{i1}^2 \sin \psi_{i1}) - \sum_{i=1}^2 \mathbf{A}_{i2} (\ddot{\psi}_{i2} \cos \psi_{i2} - \dot{\psi}_{i2}^2 \sin \psi_{i2}). \quad (8)$$

Substituting Eqs (5-7) into Eq. (8) and considering the relation $\cos^2 \alpha \sin \alpha = 0.25 \sin \alpha + 0.25 \sin 3\alpha$, one obtains:

$$\begin{aligned} F = & \mathbf{A}_{11} [\omega_0^2 \Phi_{11} (1 + 0.25 \Phi_{11}^2) \sin(\omega_0 \tau + \beta_{11}) + \omega_0^2 \Phi_{11}^3 0.25 \sin(3\omega_0 \tau + 3\beta_{11})] \\ & + \mathbf{A}_{12} [\omega_0^2 \Phi_{12} (1 + 0.25 \Phi_{12}^2) \sin(\omega_0 \tau + \beta_{12}) + \omega_0^2 \Phi_{12}^3 0.25 \sin(3\omega_0 \tau + 3\beta_{12})] \\ & + \mathbf{A}_{21} [\omega_0^2 \Phi_{21} (1 + 0.25 \Phi_{21}^2) \sin(\omega_0 \tau + \beta_{21}) + \omega_0^2 \Phi_{21}^3 0.25 \sin(3\omega_0 \tau + 3\beta_{21})] \\ & + \mathbf{A}_{22} [\omega_0^2 \Phi_{22} (1 + 0.25 \Phi_{22}^2) \sin(\omega_0 \tau + \beta_{22}) + \omega_0^2 \Phi_{22}^3 0.25 \sin(3\omega_0 \tau + 3\beta_{22})]. \end{aligned} \quad (9)$$

Equation (9) is the right-hand side of equation of the beam motion (2), hence we have:

$$\ddot{y}_b + \mathbf{K}y_b + \mathbf{C}\dot{y}_b = F. \quad (10)$$

Assuming that the damping coefficient \mathbf{C} is small, one gets:

$$\begin{aligned} y_b &= \sum_{i=1}^2 \sum_{j=1}^2 \mathbf{X}_{1ij} \mathbf{A}_{ij} \sin(\omega_0 \tau + \beta_{ij}) + \sum_{i=1}^2 \sum_{j=1}^2 \mathbf{X}_{3ij} \mathbf{A}_{ij} \sin(3\omega_0 \tau + 3\beta_{ij}), \\ \ddot{y}_b &= \sum_{i=1}^2 \sum_{j=1}^2 \mathbf{A}_{1ij} \mathbf{A}_{ij} \sin(\omega_0 \tau + \beta_{ij}) + \sum_{i=1}^2 \sum_{j=1}^2 9 \mathbf{A}_{3ij} \mathbf{A}_{ij} \sin(3\omega_0 \tau + 3\beta_{ij}), \end{aligned} \quad (11)$$

where:

$$\begin{aligned} X_{1ij} &= \frac{\omega_0^2 \Phi_{ij} (1 + 0.25 \Phi_{ij}^2)}{\mathbf{K} - \omega_0^2}, & X_{3ij} &= \frac{0.25 \omega_0^2 \Phi_{ij}^3}{\mathbf{K} - 9\omega_0^2}, \\ \mathbf{A}_{1ij} &= \frac{-\omega_0^4 \Phi_{ij} (1 + 0.25 \Phi_{ij}^2)}{\mathbf{K} - \omega_0^2}, & \mathbf{A}_{3ij} &= \frac{-0.25 \omega_0^4 \Phi_{ij}^3}{\mathbf{K} - 9\omega_0^2}. \end{aligned} \quad (12)$$

Equations (11) represent the displacement and the acceleration of the beam M , respectively.

3.2 Energy balance of the system

Multiplying Eq. (2) by the velocity of the beam \dot{y}_b , we obtain:

$$\ddot{y}_b \dot{y}_b + \mathbf{K}y_b \dot{y}_b = -\mathbf{C}\dot{y}_b^2 - \sum_{i=1}^2 \mathbf{A}_{i1} (\ddot{\psi}_{i1} \dot{y}_b \cos \psi_{i1} - \dot{\psi}_{i1}^2 \dot{y}_b \sin \psi_{i1}) - \sum_{i=1}^2 \mathbf{A}_{i2} (\ddot{\psi}_{i2} \dot{y}_b \cos \psi_{i2} - \dot{\psi}_{i2}^2 \dot{y}_b \sin \psi_{i2}). \quad (13)$$

Assuming that the motion of the pendulum is periodic with the period T ($T = 2\pi/\omega_0$) and integrating Eq. (13), we obtain the following energy balance:

$$\int_0^T \ddot{y}_b \dot{y}_b d\tau + \int_0^T \mathbf{K}y_b \dot{y}_b d\tau = - \int_0^T \mathbf{C}\dot{y}_b^2 d\tau - \int_0^T \sum_{j=1}^2 \left(\sum_{i=1}^2 \mathbf{A}_{ij} (\ddot{\psi}_{ij} \cos \psi_{ij} - \dot{\psi}_{ij}^2 \sin \psi_{ij}) \right) \dot{y}_b d\tau. \quad (14)$$

The left-hand side of Eq. (14) represents an increase in the total energy of the beam which for the periodic oscillations is equal to zero:

$$\int_0^T \ddot{y}_b \dot{y}_b d\tau + \int_0^T \mathbf{K} y_b \dot{y}_b d\tau = 0. \quad (15)$$

The first component of the right-hand side of Eq. (14) represents the energy dissipated by the linear damper \mathbf{C} :

$$W_{beam}^{DAMP} = \int_0^T \mathbf{C} \dot{y}_b^2 d\tau, \quad (16)$$

whereas the second component represents the work performed by horizontal components of the force with which the double pendula act on the beam causing its motion:

$$W_{beam}^{DRIVE} = - \int_0^T \sum_{j=1}^2 \left(\sum_{i=1}^2 \mathbf{A}_{ij} (\ddot{\psi}_{ij} \cos \psi_{ij} - \dot{\psi}_{ij}^2 \sin \psi_{ij}) \right) \dot{y}_b d\tau. \quad (17)$$

Substituting Eqs (16) and (17) into Eq. (14), we get:

$$W_{beam}^{DRIVE} - W_{beam}^{DAMP} = 0. \quad (18)$$

Multiplying the equation of the upper pendulum (Eq. (3)) by the velocity $\dot{\psi}_{i1}$, we obtain:

$$\begin{aligned} \delta_{i1} \ddot{y}_b \dot{\psi}_{i1} \cos \psi_{i1} + \mathbf{L}_{i1} \ddot{\psi}_{i1} \dot{\psi}_{i1} + \mathbf{L}_{i3} \ddot{\psi}_{i2} \dot{\psi}_{i1} \cos(\psi_{i1} - \psi_{i2}) &= -\mathbf{L}_{i3} \dot{\psi}_{i1} \dot{\psi}_{i2}^2 \sin(\psi_{i1} - \psi_{i2}) \\ -\mathbf{G}_{i1} \dot{\psi}_{i1} \sin(\psi_{i1}) - \mathbf{C}_{vdp} (1 - \mu \dot{\psi}_{i1}^2) \dot{\psi}_{i1}^2 + \mathbf{C}_{i2} (\dot{\psi}_{i2} - \dot{\psi}_{i1}) \dot{\psi}_{i1}. \end{aligned} \quad (19)$$

Assuming that the oscillations of the pendula are periodic with the period T and integrating Eq. (19), one obtains the following energy balance:

$$\begin{aligned} \int_0^T \mathbf{L}_{i1} \ddot{\psi}_{i1} \dot{\psi}_{i1} d\tau + \int_0^T \mathbf{G}_{i1} \dot{\psi}_{i1} \sin \psi_{i1} d\tau &= - \int_0^T \delta_{i1} \ddot{y}_b \dot{\psi}_{i1} \cos \psi_{i1} d\tau \\ - \int_0^T \mathbf{L}_{i3} (\dot{\psi}_{i1} \dot{\psi}_{i2}^2 \sin(\psi_{i1} - \psi_{i2}) + \ddot{\psi}_{i2} \dot{\psi}_{i1} \cos(\psi_{i1} - \psi_{i2})) d\tau &- \\ \int_0^T \mathbf{C}_{vdp} \dot{\psi}_{i1}^2 d\tau + \int_0^T \mathbf{C}_{vdp} \mu \dot{\psi}_{i1}^2 \dot{\psi}_{i1}^2 d\tau + \int_0^T \mathbf{C}_{i2} \dot{\psi}_{i2} \dot{\psi}_{i1} d\tau &- \int_0^T \mathbf{C}_{i2} \dot{\psi}_{i1}^2 d\tau. \end{aligned} \quad (20)$$

The left side of Eq. (20) represents the total energy of the upper pendula, which in the case of periodic oscillations is equal to zero:

$$\int_0^T \mathbf{L}_{i1} \ddot{\psi}_{i1} \dot{\psi}_{i1} d\tau + \int_0^T \mathbf{G}_{i1} \dot{\psi}_{i1} \sin \psi_{i1} d\tau = 0. \quad (21)$$

The first component of the right side of Eq. (20) represents the energy which is transferred to the beam:

$$W_{i1}^{SYN} = \int_0^T \delta_{i1} \ddot{y}_b \dot{\psi}_{i1} \cos \psi_{i1} d\tau. \quad (22)$$

The second component describes the energy which is transferred to the lower pendulum:

$$W_{i1}^{SYN P} = - \int_0^T \mathbf{L}_{i3}(\dot{\psi}_{i1}\dot{\psi}_{i2}^2 \sin(\psi_{i1} - \psi_{i2}) + \ddot{\psi}_{i2}\dot{\psi}_{i1} \cos(\psi_{i1} - \psi_{i2}))d\tau, \quad (23)$$

and the third component describes the energy which is supplied to the system by the van der Pol damper in one-period oscillations:

$$W_{i1}^{DAMP} = - \int_0^T (\mathbf{C}_{vdp} + \mathbf{C}_{i2})\dot{\psi}_{i1}^2 - \mathbf{C}_{i2}\dot{\psi}_{i2}\dot{\psi}_{i1}d\tau. \quad (24)$$

Finally, the last component represents the energy dissipated by the van der Pol damper:

$$W_{i1}^{SELF} = - \int_0^T \mu \mathbf{C}_{vdp}\dot{\psi}_{i1}^2 d\tau, \quad (25)$$

Substituting Eqs (22 - 25) into Eq. (20), we obtain the following relation:

$$W_{i1}^{SYN P} - W_{i1}^{SYN} + W_{i1}^{SELF} + W_{i1}^{DAMP} = 0,$$

Multiplying the equation of the lower pendulum (Eq. (4)) by the velocity $\dot{\psi}_{i2}$, one gets:

$$\begin{aligned} \delta_{i2}\ddot{y}_b\dot{\psi}_{i2} \cos \psi_{i2} + \mathbf{L}_{i3}\ddot{\psi}_{i1}\dot{\psi}_{i2} \cos(\psi_{i1} - \psi_{i2}) + \mathbf{L}_{i2}\dot{\psi}_{i2}\ddot{\psi}_{i2} = \\ \mathbf{L}_{i3}\dot{\psi}_{i1}^2\dot{\psi}_{i2} \sin(\psi_{i1} - \psi_{i2}) - \mathbf{G}_{i2}\dot{\psi}_{i2} \sin(\psi_{i2}) - \mathbf{C}_{i2}(\dot{\psi}_{i2} - \dot{\psi}_{i1})\dot{\psi}_{i2}. \end{aligned} \quad (26)$$

Assuming that the oscillations of the pendulum are periodic with the period T , the integration of Eq. (26) gives the following energy balance:

$$\begin{aligned} \int_0^T \mathbf{L}_{i2}\dot{\psi}_{i2}\ddot{\psi}_{i2}d\tau + \int_0^T \mathbf{G}_{i2}\dot{\psi}_{i2} \sin(\psi_{i2})d\tau = - \int_0^T \beta_{i2}\ddot{y}_b\dot{\psi}_{i2} \cos \psi_{i2}d\tau - \\ \int_0^T \mathbf{L}_{i3}(\dot{\psi}_{i1}^2\dot{\psi}_{i2} \sin(\psi_{i1} - \psi_{i2}) - \ddot{\psi}_{i1}\dot{\psi}_{i2} \cos(\psi_{i1} - \psi_{i2}))d\tau - \int_0^T \mathbf{C}_{i2}\dot{\psi}_{i2}^2d\tau + \int_0^T \mathbf{C}_{i2}\dot{\psi}_{i1}\dot{\psi}_{i2}d\tau. \end{aligned} \quad (27)$$

The left side of Eq. (27) represents the total energy of the lower pendulum, which in the case of periodic oscillations is equal to zero:

$$\int_0^T \mathbf{L}_{i2}\dot{\psi}_{i2}\ddot{\psi}_{i2}d\tau + \int_0^T \mathbf{G}_{i2}\dot{\psi}_{i2} \sin(\psi_{i2})d\tau = 0. \quad (28)$$

The first component of the right side of Eq. (27) represents the energy which is transferred to the beam via the upper pendulum or to the next pendulum via the upper pendulum and the beam:

$$W_{i2}^{SYN} = \int_0^T \delta_{i2}\ddot{y}_b\dot{\psi}_{i2} \cos \psi_{i2}d\tau. \quad (29)$$

The second component describes the energy which is transferred to the upper pendulum:

$$W_{i2}^{SYN P} = - \int_0^T \mathbf{L}_{i3} (\dot{\psi}_{i1}^2 \dot{\psi}_{i2} \sin(\psi_{i1} - \psi_{i2}) - \ddot{\psi}_{i1} \dot{\psi}_{i2} \cos(\psi_{i1} - \psi_{i2})) d\tau. \quad (30)$$

and the last component represents the energy dissipated by the damper:

$$W_{i2}^{DAMP} = - \int_0^T \mathbf{C}_{i2} (\dot{\psi}_{i2} - \dot{\psi}_{i1}) \dot{\psi}_{i2} d\tau \quad (31)$$

Substituting Eqs (29 - 31) into Eq. (27), one obtains the following relation:

$$W_{i2}^{SYN P} - W_{i2}^{SYN} + W_{i2}^{DAMP} = 0.$$

3.3 Energy transfer between the upper and lower pendula

The energy transferred from the upper to lower pendulum is given by:

$$W_{i1}^{SYN P} = - \int_0^T \mathbf{L}_{i3} (\ddot{\psi}_{i2} \cos(\psi_{i1} - \psi_{i2}) + \dot{\psi}_{i2}^2 \sin(\psi_{i1} - \psi_{i2})) \dot{\psi}_{i1} d\tau, \quad (32)$$

and the energy transferred from the lower to upper pendulum is:

$$W_{i2}^{SYN P} = - \int_0^T \mathbf{L}_{i3} (\ddot{\psi}_{i1} \cos(\psi_{i1} - \psi_{i2}) - \dot{\psi}_{i1}^2 \sin(\psi_{i1} - \psi_{i2})) \dot{\psi}_{i2} d\tau. \quad (33)$$

Taking into account Eqs (5 - 7), Eq. (33) takes the form:

$$\begin{aligned} W_{i1}^{SYN P} &= -\mathbf{L}_{i3} \int_0^T (-\omega_0^2 \Phi_{i2} \sin(\omega_0 t + \beta_{i2}) \cos(\Phi_{i1} \sin(\omega_0 t + \beta_{i1}) - \Phi_{i2} \sin(\omega_0 t + \beta_{i2})) \\ &+ \omega_0^2 \Phi_{i2}^2 \cos^2(\omega_0 t + \beta_{i2}) \sin(\Phi_{i1} \sin(\omega_0 t + \beta_{i1}) - \Phi_{i2} \sin(\omega_0 t + \beta_{i2}))) \omega_0 \Phi_{i1} \cos(\omega_0 t + \beta_{i1}) d\tau \\ &= \mathbf{L}_{i3} \pi \omega_0^2 \Phi_{i1} \Phi_{i2} \sin(\beta_{i2} - \beta_{i1}), \end{aligned} \quad (34)$$

and

$$W_{i2}^{SYN P} = \mathbf{L}_{i3} \pi \omega_0^2 \Phi_{i1} \Phi_{i2} \sin(\beta_{i1} - \beta_{i2}) = -W_{i1}^{SYN P}, \quad (35)$$

The synchronization between the lower and upper pendula occurs when:

$$W_{i1}^{SYN P} = 0 \quad \Rightarrow \quad \sin(\beta_{i1} - \beta_{i2}) = 0. \quad (36)$$

Condition (36) is fulfilled when:

$$\beta_{i1} = \beta_{i2} \vee (\beta_{i1} = 0 \wedge \beta_{i2} = \pi). \quad (37)$$

In the first case, the oscillations of the upper and lower pendula are in-phase, i.e., the pendula move in the same directions, whereas in the second case they are in anti-phase, i.e., the pendula move in the opposite directions. For low oscillations, limit conditions (37) define two normal modes of oscillations [1].

3.4 Synchronization of the double pendula

In each equation of the pendulum motion, there is a component influencing the beam motion

$$M_{ij}^{SYN} = \delta_{ij} \ddot{y}_b \cos \psi_{ij}, \quad (38)$$

which is called the synchronization momentum (torque). The work done by this momentum during one period is equal to zero.

$$W_{ij}^{SYN} = \int_0^T \delta_{ij} \ddot{y}_b \cos \psi_{ij} \dot{\psi}_{ij} d\tau = 0. \quad (39)$$

Substituting Eqs (5, 6) and (11) into (39) and performing the linearization, we arrive at:

$$\begin{aligned} W_{11}^{SYN} &= \int_0^T \delta_{11} \left(\sum_{i=1}^2 \sum_{j=1}^2 \mathbf{A}_{1ij} \mathbf{A}_{ij} \sin(\omega_0 t + \beta_{ij}) + \sum_{i=1}^2 \sum_{j=1}^2 \mathbf{A}_{3ij} \mathbf{A}_{ij} \sin(3\omega_0 t + 3\beta_{ij}) \right) \omega_0 \Phi_{11} \cos(\omega_0 t + \beta_{11}) d\tau = \\ &= \delta_{11} \omega_0 \pi \Phi_{11} \sum_{i=1}^2 \sum_{j=1}^2 \mathbf{A}_{1ij} \mathbf{A}_{ij} \sin(\beta_{ij} - \beta_{11}) = \\ &= \xi \delta_{11} \Phi_{11} \left[\sum_{i=1}^2 \sum_{j=1}^2 \Theta_{ij} M_{ij} \sin(\beta_{ij} - \beta_{11}) \right] = 0, \\ W_{12}^{SYN} &= \xi \delta_{12} \Phi_{12} \left[\sum_{i=1}^2 \sum_{j=1}^2 \Theta_{ij} M_{ij} \sin(\beta_{ij} - \beta_{12}) \right] = 0, \\ W_{21}^{SYN} &= \xi \delta_{21} \Phi_{21} \left[\sum_{i=1}^2 \sum_{j=1}^2 \Theta_{ij} M_{ij} \sin(\beta_{ij} - \beta_{21}) \right] = 0, \\ W_{22}^{SYN} &= \xi \delta_{22} \Phi_{22} \left[\sum_{i=1}^2 \sum_{j=1}^2 \Theta_{ij} M_{ij} \sin(\beta_{ij} - \beta_{22}) \right] = 0, \end{aligned} \quad (40)$$

where:

$$\xi = \frac{-\omega_0^5 \pi}{M l_b (\mathbf{K} - \omega_0^2)}, \quad M_{i1} = (m_{i1} + m_{i2}) l_{i1}, \quad M_{i2} = m_{i2} l_{i2}, \quad \Theta_{ij} = \Phi_{ij} (1 + 0.25 \Phi_{ij}^2). \quad (41)$$

Equations (40) allow the calculation of the phase angles β_{ij} for which the synchronization of periodic oscillations of the pendula occurs. The synchronization occurs when the following equations are fulfilled:

$$\begin{aligned} \Theta_{12} M_{12} \sin(\beta_{12} - \beta_{11}) + \Theta_{21} M_{21} \sin(\beta_{21} - \beta_{11}) + \Theta_{22} M_{22} \sin(\beta_{22} - \beta_{11}) &= 0, \\ \Theta_{11} M_{11} \sin(\beta_{11} - \beta_{12}) + \Theta_{21} M_{21} \sin(\beta_{21} - \beta_{12}) + \Theta_{22} M_{22} \sin(\beta_{22} - \beta_{12}) &= 0, \\ \Theta_{11} M_{11} \sin(\beta_{11} - \beta_{21}) + \Theta_{12} M_{12} \sin(\beta_{12} - \beta_{21}) + \Theta_{22} M_{22} \sin(\beta_{22} - \beta_{21}) &= 0, \\ \Theta_{11} M_{11} \sin(\beta_{11} - \beta_{22}) + \Theta_{12} M_{12} \sin(\beta_{12} - \beta_{22}) + \Theta_{21} M_{21} \sin(\beta_{21} - \beta_{22}) &= 0. \end{aligned} \quad (42)$$

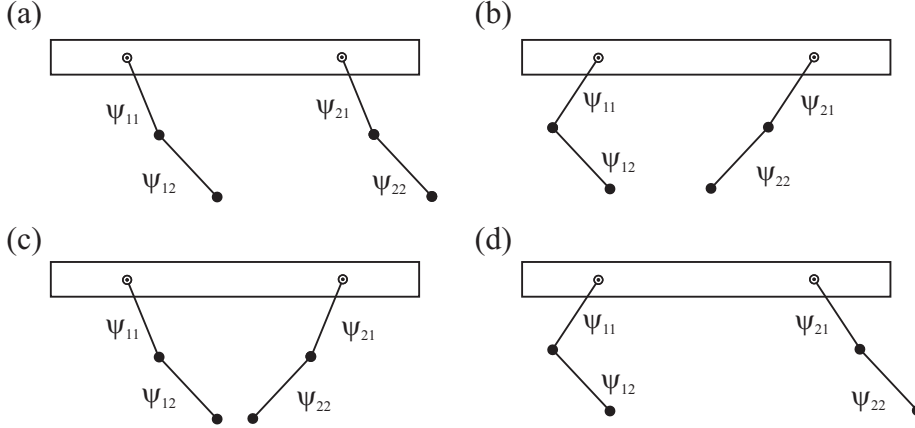


Fig. 2. Synchronous states of the system (1): (a) upper and lower pendula in phase: $\psi_{11} = \psi_{21}$ and $\psi_{12} = \psi_{22}$, (b) upper pendula in phase, lower pendula in anti-phase: $\psi_{11} = \psi_{21}$ and $\psi_{12} = -\psi_{22}$, (c) upper and lower pendula in anti-phase: $\psi_{11} = -\psi_{21}$ and $\psi_{12} = -\psi_{22}$ (d) upper pendula in anti-phase, lower pendula in phase: $\psi_{11} = -\psi_{21}$ and $\psi_{12} = \psi_{22}$.

Equations (42) are fulfilled for β_{ij} , which are combinations of 0 and π . Assuming that $\beta_{11} = 0$, one can identify the following pendulum configurations which are presented in Fig. 2(a-d). The first type is the configuration shown in Fig. 2(a). Both the upper and lower pendula are phase synchronized, i.e., $\psi_{11} = \psi_{21}$ and $\psi_{12} = \psi_{22}$ ($\beta_{11} = \beta_{12} = \beta_{21} = \beta_{22} = 0$ or $\beta_{11} = \beta_{21} = 0$, $\beta_{12} = \beta_{22} = \pi$). The upper and lower pendula are synchronized in phase and anti-phase, respectively, i.e., $\psi_{11} = \psi_{21}$ and $\psi_{12} = -\psi_{22}$ in the configuration from Fig. 2(b) ($\beta_{11} = \beta_{12} = \beta_{21} = 0$, $\beta_{22} = \pi$ or $\beta_{11} = \beta_{12} = \beta_{22} = 0$, $\beta_{21} = \pi$). Figure 2(c) presents the case when both the upper and lower pendula are synchronized in anti-phase, i.e., $\psi_{11} = -\psi_{21}$ and $\psi_{12} = -\psi_{22}$ ($\beta_{11} = \beta_{12} = 0$, $\beta_{21} = \beta_{22} = \pi$ or $\beta_{11} = \beta_{22} = 0$, $\beta_{12} = \beta_{21} = \pi$). Finally, in Fig. 2(d), we present the case when the upper pendula are in anti-phase and the lower pendula are in phase $\psi_{11} = -\psi_{21}$ and $\psi_{12} = \psi_{22}$ ($\beta_{11} = \beta_{12} = \beta_{22} = 0$, $\beta_{21} = \pi$ or $\beta_{11} = 0$, $\beta_{21} = \beta_{12} = \beta_{22} = \pi$).

4 Numerical investigations

In our numerical calculations, we use the Auto 07p [29] continuation toolbox to obtain periodic solutions. To start path-following, we integrate Eqs (2-4) with the fourth-order Runge-Kutta method. We consider the following parameter values: $m_{11} = m_{12} = m_{21} = m_{22} = 1.0$ [kg], $M = 10.0$ [kg], $l_{11} = l_{12} = l_{21} = l_{22} = 0.2485$ [m], $k_x = 4.0$ [N/m], $c_x = 1.53$ [Ns/m], $c_{vdp} = -0.1$ [Ns/m], $\mu = 60.0$ [m⁻²], $c_{i2} = 0.0016$ [Ns/m], which yield the following dimensionless coefficients $\mathbf{A}_{i1} = 0.0354986$, $\mathbf{A}_{i2} = 0.01774933$, $\delta_{i1} = 0.142857$, $\delta_{i2} = 0.0714286$, $\mathbf{L}_{i1} = 0.035986$, $\mathbf{L}_{i2} = 0.0177493$, $\mathbf{L}_{i3} = 0.0177493$, $\mathbf{G}_{i1} = 0.0354986$, $\mathbf{G}_{i2} = 0.0177493$, $\mathbf{C}_{vdp} = -0.00457491$, $\mathbf{C}_{i2} = 0.0000714286$, $\mathbf{C} = 0.0173934$, $\mathbf{K} = 0.00723723$. Our bifurcation parameters are masses of the pendula and the beam. To hold an intuitive physical interpretation, we change dimensional masses, but all the calculation are performed for dimensionless equations.

4.1 Periodic solutions to the pendula with identical masses

Depending on the initial conditions, we observe four different synchronous states of system (2-4) as shown in Fig. 3(a-d). The in-phase motion is represented by two periodic solutions: the first type is characterized by a lack of phase differences in the pendulum angular positions: $\beta_{11} = \beta_{21} = \beta_{12} = \beta_{22}$ (see Fig. 3(a)), whereas the second one - by a phase difference between the upper and lower pendula in each double pendulum: $\beta_{11} = \beta_{21}$, $\beta_{12} = \beta_{22}$ and $\beta_{i1} - \beta_{i2} = \pi$, $i = 1, 2$ (see Fig. 3(b)). In both cases, the displacements of the upper and lower pendula of each double pendulum are identical, i.e., $\psi_{11} = \psi_{21}$, $\psi_{12} = \psi_{22}$. The beam motion is in anti-phase to the upper pendula and in-phase (Fig. 3(a)) or anti-phase (Fig. 3(b)) to the lower ones. These two configurations correspond to the analytically predicted synchronous state presented in Fig. 2(a). The second type, the anti-phase motion, for which the beam is not moving, is shown in Fig. 3(c,d). We can also distinguish two types of this periodic solution, both characterized by the following phase differences of the pendulum displacements: $\beta_{11} - \beta_{21} = \pi$ and $\beta_{12} - \beta_{22} = \pi$, but different phase shifts between the pendula in each double pendulum: $\beta_{i1} - \beta_{i2} = \pi$, $i = 1, 2$ (see Fig. 3(c)) and $\beta_{i1} - \beta_{i2} = 0$, $i = 1, 2$ (see Fig. 3(d)). The beam M is at rest, because reaction forces acting on the beam are vanishing. These pendulum configurations correspond to the theoretically predicted synchronous state presented in Fig. 2(c). Note that for this type of the synchronous state, amplitudes of pendulum oscillations can be estimated analytically. Substituting $\beta_{11} = \beta_{12} = 0$ and $\beta_{21} = \beta_{22} = \pi$ in Eqs (42), one can derive an analytical formula for amplitudes of pendulum oscillations. The amplitudes of the upper pendula can be approximated by:

$$\Phi_{11} = \Phi_{21} = 2\sqrt{\frac{1}{\mu}}. \quad (43)$$

The approximate values of the amplitudes of oscillations of the lower pendula can be calculated from the following condition:

$$\begin{aligned} \frac{1}{4}\omega_0\pi(4\mathbf{C}_{i2}(\Phi_{i1}^2 + \Phi_{i2}^2) + \mathbf{C}_{vdp}\Phi_{i1}^2(4 - \mu\Phi_{i1}^2) - 8\mathbf{C}_{i2}\Phi_{i1}\Phi_{i2}\cos(\beta_{i1} - \beta_{i2}) + \\ \Phi_{i1}\Phi_{i2}(\Phi_{i2}^2 - \Phi_{i1}^2)\mathbf{L}_{i3}\omega_0\sin(\beta_{i1} - \beta_{i2})) = 0 \end{aligned} \quad (44)$$

For $i = 1, 2$, formulae (43) and (44) give good approximation of the numerical values, e.g., for the parameter values in Fig. 3(c,d), the analytically calculated amplitudes of the upper and lower pendula are $\Phi_{11} = \Phi_{21} = 0.2581$ and $\Phi_{12} = \Phi_{22} = 0.4244$, respectively, whereas the numerical values are $\Phi_{11} = \Phi_{21} = 0.2522$ and $\Phi_{12} = \Phi_{22} = 0.3536$ for Fig. 3(c) and $\Phi_{12} = \Phi_{22} = 0.2579$ and $\Phi_{11} = \Phi_{21} = 0.3732$ for Fig. 3(d). In Fig. 3(a,d), one can see that the pendula do not pass through zero (the hanging down position) at the same moment of time, whereas in Fig. 3(b,c) the pendula cross this position simultaneously. The phase shift is observed only when the lower and upper pendula in each double pendulum are oscillating in-phase with non-zero damping between them.

We do not observe the configurations shown in Fig. 2(b,d) because each of the double pendulum has to reach different normal modes of oscillations for the same frequency for both of them. This is proven to be impossible in the low oscillation approximation [1] (the angular positions have to be much higher than the one considered in this paper).

The periodic solutions presented in Fig. 3(a,b,d) are stable, whereas the one from Fig. 3(c) is unstable. To show how a change in the natural frequency of the beam affects the stability of the periodic solutions obtained, we calculate one-parameter

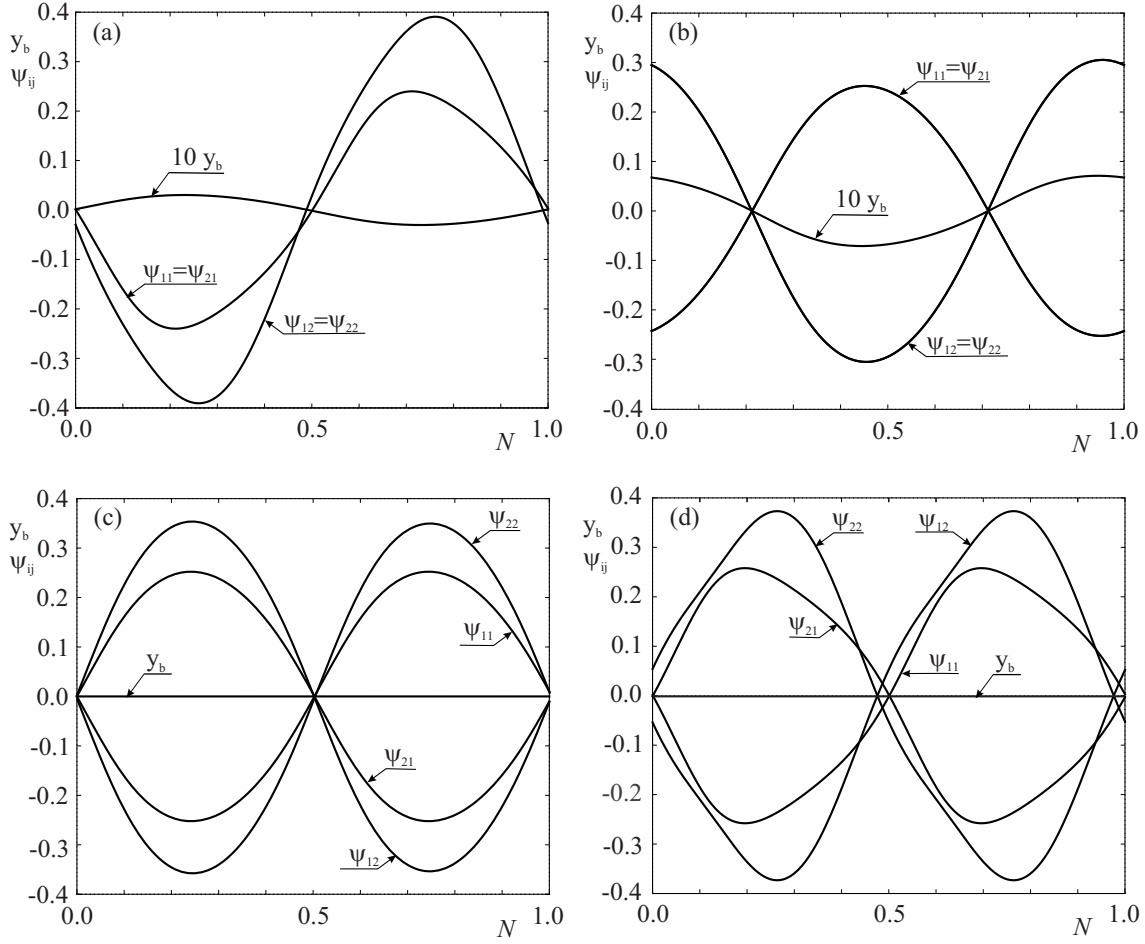


Fig. 3. Pendulum and beam displacements for one period of motion ($N = 1$) for four different periodic solutions in the case of identical masses of the pendula: $m_{11} = m_{12} = m_{21} = m_{22} = 1.0$ [kg]. The displacement y_b of the beam M is shown 10 times magnified. (a) pendulum configuration from Fig. 2(a) with the period $T = 7.233$, (b) pendulum configuration from Fig. 2(a) with the period $T = 3.362$, (c) pendulum configuration from Fig. 2(c) with the period $T = 3.748$, and (d) pendulum configuration from Fig. 2(c) with the period $T = 8.266$.

bifurcation diagrams. We choose the beam mass M as the bifurcation parameter and vary it in the range from 0.01 [kg] to 20.0 [kg]. In the case of two solutions: one in-phase (Fig. 3(b)) and one anti-phase (Fig. 3(d)), we do not observe any destabilization of periodic solutions. For the two others, we present bifurcation diagrams showing the maximum amplitudes of the beam oscillation $\max y_b$ on the vertical axes. The black and gray colors of branches correspond to stable and unstable periodic solutions. For the branch presented in Fig. 4(a), we start a continuation from the in-phase periodic solution shown in Fig. 3(a). Originally, the stable periodic orbit becomes unstable with a decreasing beam mass M in the Neimark-Sacker bifurcation for $M = 3.88$ [kg]. The Neimark-Sacker bifurcation point corresponds also to the maximum amplitude of the beam. In Fig. 4(b), we show a continuation of the anti-phase oscillations of the pendula (Fig. 3(c)). The stabilization of this type of the periodic solution occurs in the supercritical pitchfork bifurcation (two new branches

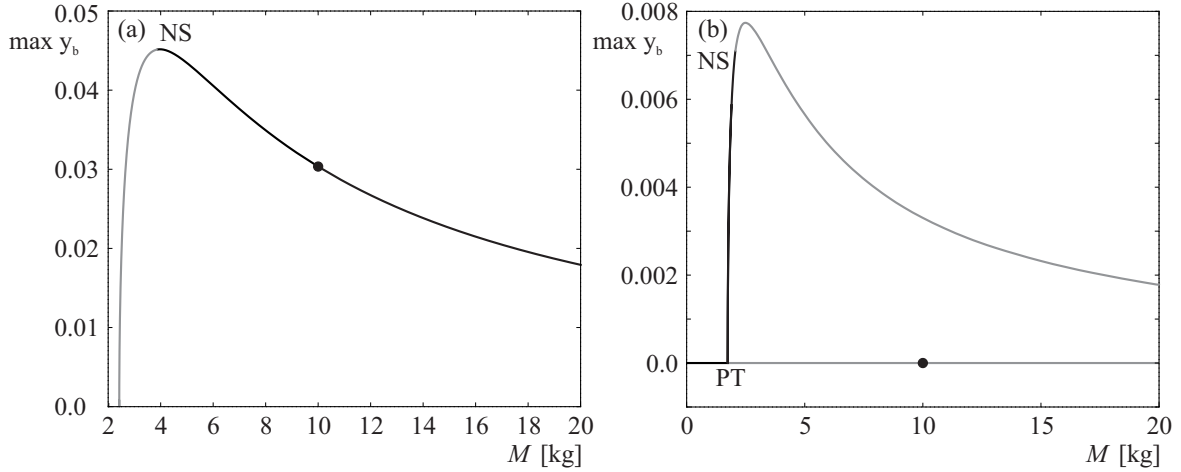


Fig. 4. One-parameter path-following of periodic solutions for the varying mass M of the beam: (a) in-phase motion from Fig. 3(a) and (b) anti-phase motion from Fig. 3(c). The black and gray lines correspond to stable and unstable periodic solutions, respectively. The abbreviation NS stands for the Neimark-Sacker bifurcation and PT denotes the pitchfork bifurcation. Bifurcations along unstable branches are neglected. The starting points of continuation are marked by black dots.

emerge) for $M = 1.737$ [kg]. In the symmetric anti-phase motion, the beam is at rest and the maximum amplitudes of the pendula remain the same. For the asymmetric periodic solutions along two overlapping branches, the beam is oscillating with a low amplitude and we observe a difference between amplitudes of the pendula. The asymmetric motion destabilizes with an increase in the beam mass M in Neimark-Sacker bifurcations for $M = 2.06$ [kg].

4.2 Periodic solutions of the pendula with different masses - exploring symmetry

In this subsection, we investigate the stability of symmetric motion of the pendula from Fig. 3(c,d), which corresponds to anti-phase synchronization states. We decrease the masses m_{12} and m_{22} of the lower pendula in the range $(0.0, 1.0)$ [kg]. We choose masses of the lower pendula as the bifurcation parameter because we want to avoid a situation where the lightweight upper pendula excite the much heavier lower pendula.

In Fig. 5(a,b) we present bifurcation diagrams, i.e., the maximum amplitudes of the beam (a) and the second upper pendulum (b) for decreasing masses of the lower pendula. As an initial state, we take the anti-phase periodic solution for which all pendula have identical masses (see Fig. 3(d)). For $m_{12} = m_{22} = 0.108$ [kg], the symmetry is broken in the subcritical pitchfork bifurcation. We observe an appearance of two unstable branches which stabilize in saddle-node bifurcations for $m_{12} = m_{22} = 0.107$ [kg], a further loss of stability occurs in the supercritical Neimark-Sacker bifurcations for $m_{12} = m_{22} = 0.105$ [kg], hence two stable quasi-periodic solutions appear. This scenario is observed only when the system has symmetry. The bifurcation diagram for a system without symmetry ($m_{11} = 1.0$ [kg] and $m_{12} = 0.99$ [kg]) is shown in Fig. 5(c,d). We present the maximum amplitudes of the upper pendula in the range $m_{i2} \in (0.0, 0.15]$ [kg] (for $m_{i2} \in (0.15, 1.0]$ [kg], solutions are stable). As can be easily predicted, the pitchfork bifurcation is no more present and we observe two disconnected branches of periodic solutions (the imperfect pitchfork bifurcation). As one can see, the maximum amplitudes of the lower pendula start to diverge close to the

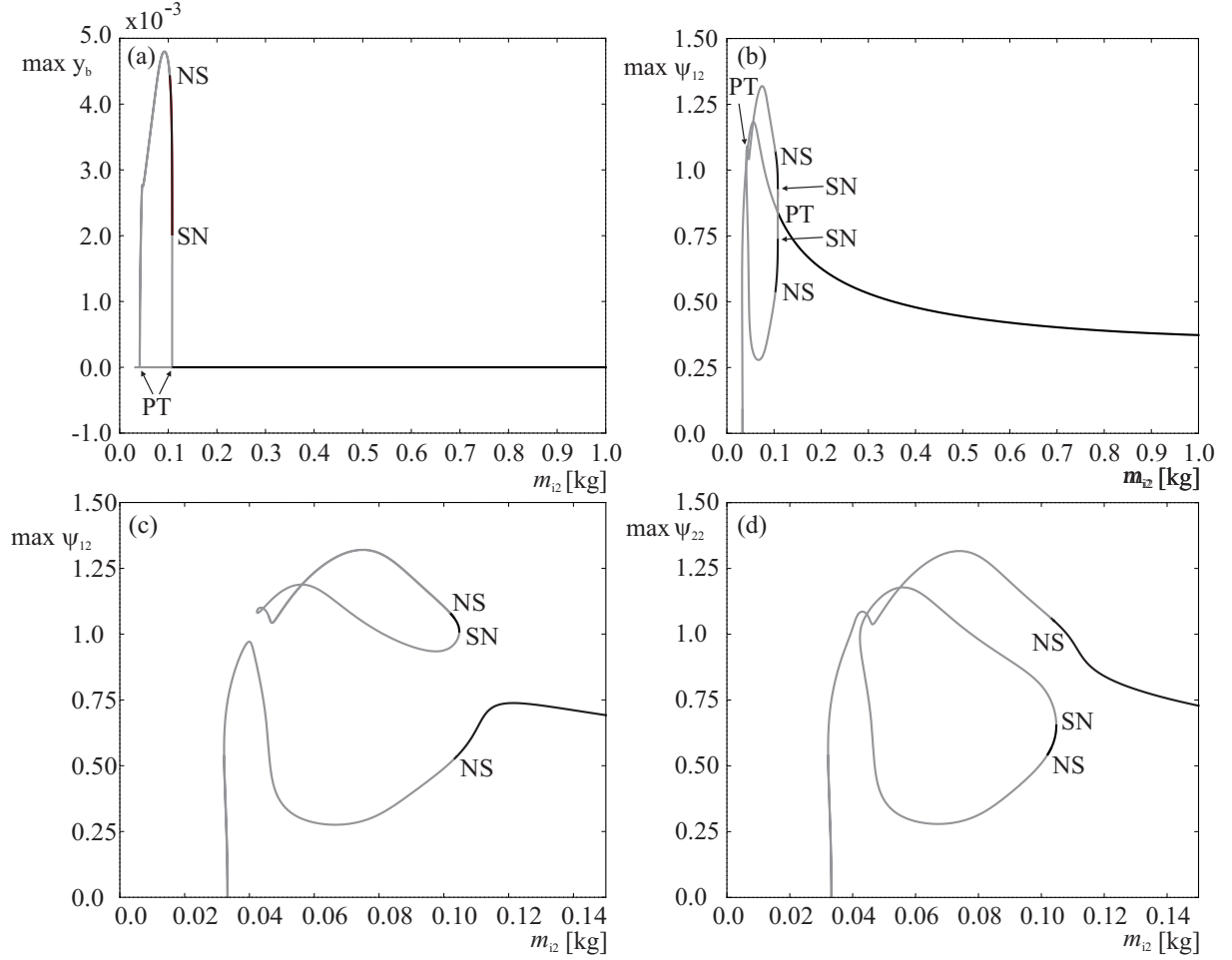


Fig. 5. In (a,b) we show one-parameter path-following of the anti-phase synchronous motion starting from the periodic solution shown in Fig. 3(d). The changes in the maximum amplitude of the beam $\max y_b$ (a) and the second upper pendulum $\max \psi_{12}$ (b) are shown for decreasing masses of the lower pendula $m_{i2} = (0.0, 1.0)$ [kg] ($i = 1, 2$), whereas the upper pendula have masses equal to 1.0 [kg]. In (c,d) the same calculations are performed for asymmetrical masses of the upper pendula ($m_{11} = 1.0$ [kg], $m_{21} = 0.99$ [kg]) in the range $m_{i2} \in (0.0, 0.15)$ [kg] ($i = 1, 2$), for $m_{i2} \in (0.15, 1.0)$ [kg] ($i = 1, 2$), solutions are stable. The black and gray lines correspond to stable and unstable periodic solutions, respectively. The abbreviations correspond to: PT - pitchfork bifurcation, NS - Neimark-Saker bifurcation, and SN - saddle-node bifurcation. Bifurcations along unstable branches are neglected.

destabilization and the second lower pendulum has nearly twice a higher amplitude than the first one in the Neimark-Saker bifurcation point ($m_{12} = m_{22} = 0.103$ [kg]). Close to the Neimark-Saker bifurcation located on the main branch, one can observe an appearance of the second branch which starts and disappears in saddle-node bifurcations. The stable part of this branch is bounded by the saddle-node ($m_{12} = m_{22} = 0.1019$ [kg]) and the Neimark-Sacker ($m_{12} = m_{22} = 0.1047$ [kg]) bifurcations and there is a similar difference in amplitudes between the lower and upper pendula as for the main branch. The stability range of this separated branch in the two-parameter space is studied in the next subsection.

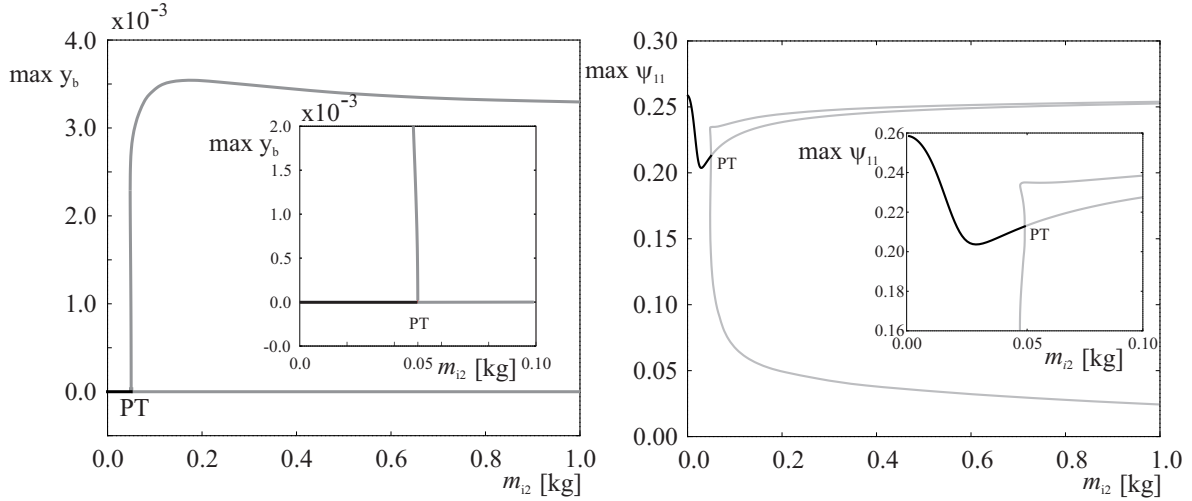


Fig. 6. One-parameter path-following of the anti-phase synchronous periodic solutions from Fig. 3(c). A change in the maximum amplitude of the beam $\max y_b$ (a) and the second upper pendulum $\max \psi_{12}$ (b) is shown for decreasing masses of the lower pendula $m_{i2} \in (0.0, 1.0)$ [kg] ($i = 1, 2$), whereas the upper pendula have masses equal to 1.0 [kg]. The black and gray lines correspond to stable and unstable periodic solutions, respectively. The abbreviation PT corresponds to the pitchfork bifurcation. Bifurcations along unstable branches are neglected.

The same analysis is performed for the periodic solution shown in Fig. 3(c), which is originally unstable. In Fig. 6(a) one can see that the maximum amplitude of the beam $\max y_b$ with decreasing masses of the lower pendula m_{12} and m_{22} remains zero (symmetry is maintained) in the whole range under consideration. For $m_{12} = m_{22} = 0.05$ [kg], we observe the subcritical pitchfork bifurcation, where symmetric solutions stabilize and stay stable nearly to $m_{12} = m_{22} \approx 0.0$ [kg]. The second branch corresponds to the asymmetric unstable periodic motion with low oscillations of the beam. All branches coming from the pitchfork bifurcation can be seen in Fig. 6(b), where we show the maximum amplitude of the second upper pendulum $\max \psi_{12}$. To have a general overview, we increase the masses m_{12} and m_{22} but the stability properties do not change, hence the periodic solutions along all branches stay unstable.

4.3 Ranges of stability of synchronous solutions in the two-parameter space

In this subsection, we show how asymmetric changes of pendulum masses influence the stability of the previously present periodic solutions. In all cases we start with the pendulum configuration obtained for the identical double pendula (configurations from Fig. 3(a-d)). We change the mass of the second upper pendulum m_{21} (in different intervals for each periodic solutions) and the masses of the lower pendula $m_{12} = m_{22}$ in the interval $(0.0, 1]$ [kg]. Our calculations are presented on the two-dimensional bifurcation diagrams (masses of the lower pendula $m_{12} = m_{22}$ versus the mass of the second upper pendulum m_{21}).

In Fig. 7(a) we show stability ranges of the configuration presented in Fig. 3(d). The solution is bounded by the Neimark-Sacker bifurcation, hence we observe an appearance of the quasi-periodic motion outside this range. The bifurcation scenario which occurs for $m_{21} = 1.0$ [kg] is different from the other ones because of the presence of symmetry. The stability at the bottom is lost not via the Neimark-Sacker but

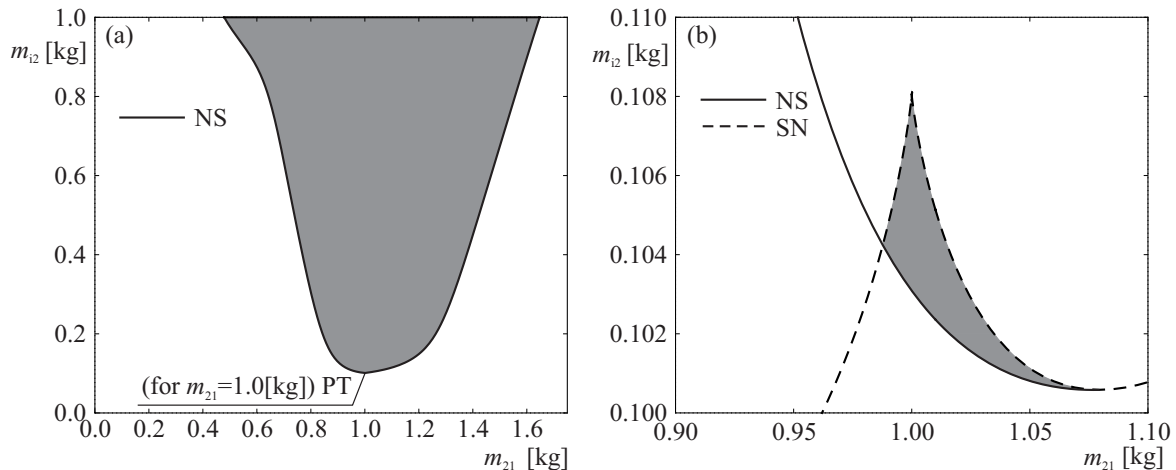


Fig. 7. In (a) two-parameter continuation of the anti-phase synchronization periodic solution (the beam is at rest - see Fig. 3(d)) for the masses m_{21} and $m_{i2} \in (0.0, 1.0]$ [kg]. The observed stable periodic solutions destabilize through the Neimark-Sacker bifurcations. When the system is symmetric ($m_{21} = 1.0$ [kg]), the Neimark-Sacker bifurcation is interchanged by the pitchfork bifurcation. In (b) two-parameter plot for the masses m_{21} and $m_{i2} \in (0.0, 1.0]$ [kg] of the disconnected branch (see Fig. 5(c,d)). Stable periodic solutions destabilize through the Neimark-Sacker (continuous line) and saddle-node (dashed line) bifurcations. The gray shaded area corresponds to the existence of stable periodic solutions, whereas the white one to the unstable solution.

through the pitchfork bifurcation. When the symmetry is broken ($m_{21} \neq 1.0$ [kg]), the pitchfork bifurcation is no more present but there exists a disconnected stable range of periodic solutions (coming from the 'second' branch - see Fig. 5(c,d)). The area of existence of these asymmetric period solutions is presented in Fig. 7(b). As shown in Fig. 5(c,d), the stable range is bounded by the Neimark-Sacker bifurcation (from the bottom) and the saddle-node bifurcation line from the top. This area is small and when the difference of masses of the upper pendula (m_{11} and m_{21}) becomes larger than a few percent, it disappears.

One can distinguish two types of the in-phase motion: the first one where all pendula are in-phase (Fig. 3(a)) and the second one where the upper and lower pendula are in-phase but in anti-phase to each other (Fig. 3(b)). To investigate the first type of motion, we follow the periodic solution in the two-parameter space (similarly as for the anti-phase motion). The results of calculations are presented in Fig. 8(a,b). As can be easily seen, the stable area is much larger than in the previous case. Solutions destabilize similarly in the Neimark-Sacker bifurcations, which results in an appearance of the quasi-periodic motion. For a decreasing mass m_{21} , we observe a rapid jump around $m_{21} = 0.5$ [kg] from $m_{i2} \approx 0.08$ [kg] to $m_{i2} \approx 0.7$ [kg], for an increase in m_{21} , the bound of bifurcation grows nearly linearly reaching $m_{i2} = 1.0$ [kg] for $m_{21} = 4.6$ [kg]. The zoom of the majority of the left part is presented in 8(b), where one can see that the Neimark-Sacker bifurcation line has a complex structure. The gap for m_{i2} corresponds to an appearance of the quasi-periodic motion in the Neimark-Sacker bifurcation and its disappearance in the inverse Neimark-Sacker bifurcation.

In Fig. 8(c) we present a one-parameter plot which shows a connection between the unstable anti-phase solution (Fig. 3(c)) and the stable in-phase solution (Fig. 3(b)). The starting solution is the unstable one ($m_{21} = 1.0$ [kg] and $\max y_b = 0.0$) with an increasing mass, we do not observe changes in stability - the unstable branch

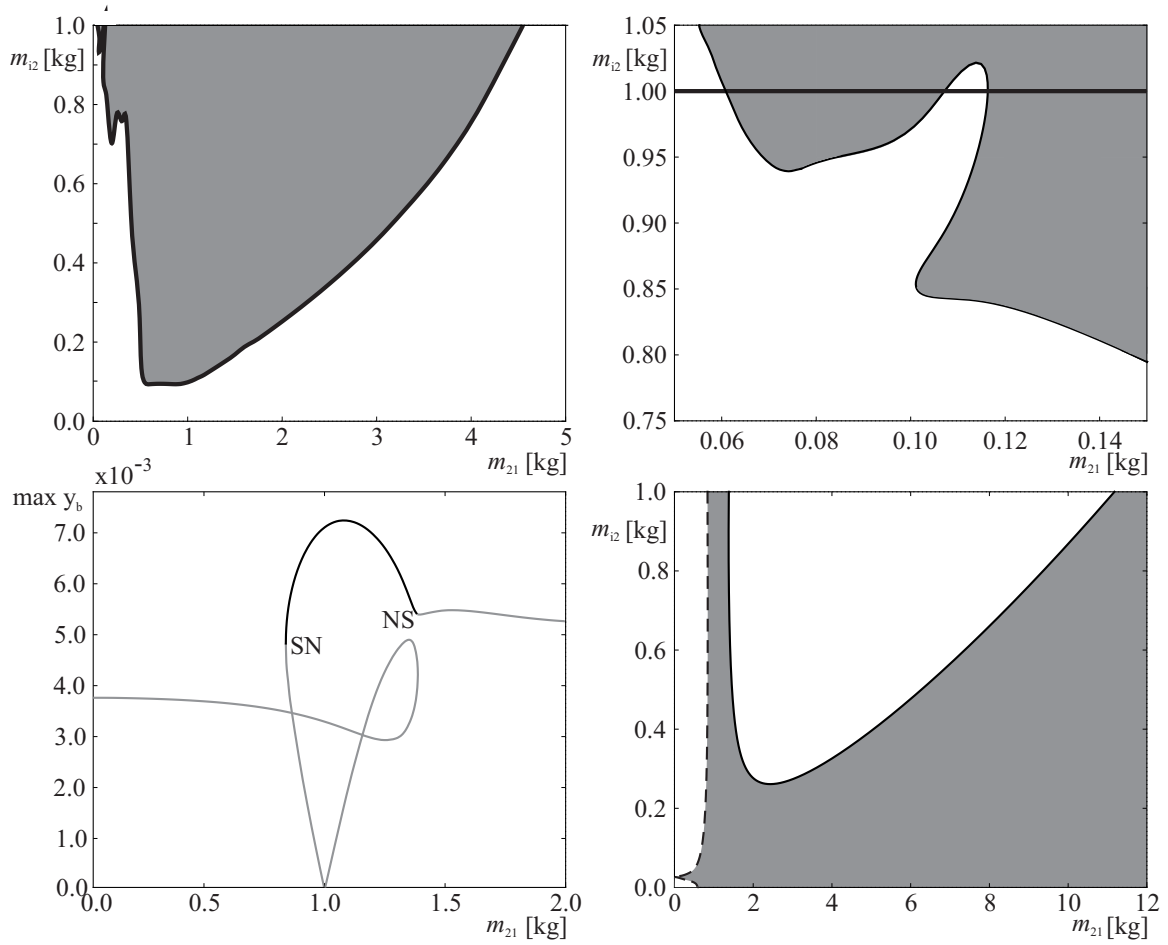


Fig. 8. In (a,b) two-parameter continuation of the in-phase synchronization periodic solution (the beam is in the anti-phase state to all pendula) for the masses m_{21} and $m_{i2} \in (0.0, 1.0]$ [kg]. The observed stable periodic solutions destabilize through the Neimark-Sacker bifurcation. In (c) one-parameter (m_{21}) plot which shows the connection between the unstable anti-phase solution (Fig. 3(c)) and the stable in-phase solution (Fig. 3(b)), where the gray and black lines correspond to stable and unstable periodic solutions. Then, in (d) two-parameter plot for the masses m_{21} and $m_{i2} \in (0.0, 1.0]$ [kg]. Stable periodic solutions destabilize through the Neimark-Sacker (continuous line) and saddle-node (dashed line) bifurcations. The gray shaded area corresponds to the existence of stable periodic solutions, whereas the white one to the unstable solution.

turns around and reaches $m_{i2} \approx 0.0$ [kg]. Following the second direction results in a change of stability in the saddle-node bifurcation ($m_{21} = 0.837$ [kg]) and then destabilization in the Neimark-Sacker bifurcation ($m_{21} = 1.38$ [kg]). For $m_{21} = 1.0$ [kg], the stable solution corresponds to the solution presented in Fig. 3(b). Next, we follow the bifurcation which bounds the stable branch in the two-parameter space (m_{21} and m_{i2}), which is shown in Fig. 8(d). The stable range stays narrow up to $m_{i2} \approx 0.3$ [kg] where the Neimark-Sacker bifurcation line changes the direction and starts to go up. When the mass of the upper pendulum is large enough ($m_{21} > 11.0$ [kg]), we once again can observe a stable solution for $m_{i2} = 1.0$ [kg]. From the left-hand side, as has

been mentioned before, the stable area is bounded by the saddle-node bifurcation line and is nearly a constant line around $m_{21} = 0.84$ [kg].

5 Conclusions

Our studies show that two self-excited double pendula with the van der Pol type of damping, hanging from the horizontally movable beam, can synchronize. For identical pendula, four different synchronous configurations are possible (in-phase or anti-phase), but not all of them are stable for the given parameters of the beam. When the pendula are nonidentical, i.e., have different masses, we observe synchronous states for which the phase difference between the pendula is close to 0 or π for a small parameter mismatch. With an increase in this difference, we observe a stable solution with phase shifts between 0 and π . They finally destabilize in the Neimark-Sacker saddle-node bifurcations, which results in an appearance of unsynchronized quasi-periodic oscillations or a jump to another attractor. Similar synchronous states have been observed experimentally in [28] but a special controlling procedure has been applied to stabilize them.

The observed behavior of system (1) can be explained by the energy expressions derived in Section 3, which also show why other synchronous states are not possible. We prove that the observed behavior of the system is robust as it occurs in a wide range of system parameters.

Acknowledgment

This work has been supported by the Foundation for Polish Science, Team Programme under the project TEAM/2010/5/5.

References

References

1. A. Andronov, A. Witt, S. Khaikin, *Theory of Oscillations*. (Pergamon, Oxford 1966)
2. I.I. Blekhman, *Synchronization in Science and Technology*. (ASME, New York 1988).
3. A. Pikovsky, M. Roesenblum, J. Kurths, *Synchronization: An Universal Concept in Nonlinear Sciences*. (Cambridge University Press, Cambridge 2001).
4. M. P. Aghababa, H. P. Aghababa, *Nonlinear Dynamics* **67**, 2689, (2012).
5. M. Kapitaniak, P. Brzeski, K. Czolczynski, P. Perlikowski, A. Stefanski and T. Kapitaniak, *Progress of Theoretical Physics* **128**(6), 1141,(2012).
6. C. Huygens, 1893, Letter to de Sluse, In: *Oeuvres Completes de Christian Huygens*, (letters; no. 1333 of 24 February 1665, no. 1335 of 26 February 1665, no. 1345 of 6 March 1665), (Societe Hollandaise Des Sciences, Martinus Nijhoff, La Haye).
7. M. Kapitaniak, K. Czolczynski, P. Perlikowski, A. Stefanski, T. Kapitaniak, *Physics Report* **517**, 1, (2012).
8. M. Bennet, M.F. Schatz, H., Rockwood, K. Wiesenfeld, *Proc. Roy. Soc. London A* **458**, 563, (2002).
9. K. Czolczynski, P. Perlikowski, A. Stefanski, T. Kapitaniak, *Prog. Theor. Phys.* **122**, 1027, (2009).
10. K. Czolczynski, P. Perlikowski, A. Stefanski, T. Kapitaniak, *Physica A* **388**, 5013, (2009).
11. K. Czolczynski, P. Perlikowski, A. Stefanski, T. Kapitaniak, *Chaos* **21**, 023129, (2011).
12. R. Dilao, *Chaos* **19**, 023118 (2009).

13. A.L. Fradkov, B. Andrievsky, *Int. J. Non-linear Mech.* **42**, 895, (2007).
14. A. Yu. Kanunnikov , R.E. Lamper, *J. Appl. Mech & Theor. Phys.* **44**, 748, (2003).
15. J. Pantaleone, *Am. J. Phys.* **70**, 992 (2002).
16. P. Perlikowski, M. Kapitaniak, K. Czolczynski, A. Stefanski, T. Kapitaniak, *Int. J. Bif. Chaos* **22**, 1250288 (2012)
17. M. Senator, *Journal Sound and Vibration*, **291**, 566, (2006).
18. H. Ulrichs, A. Mann, U. Parlitz, *Chaos* **19**, 043120 (2009).
19. N. Rott, *Z. angew. Math. Phys.* **21**, 570, (1970).
20. J. Miles, *Journal of Applied Mathematics and Physics (ZAMP)* **36**, (1985)
21. A.C. Skeldon, *Physics Letters A* **166**, 224, (1992)
22. A.C. Skeldon, *Physica D* **75**, 541, (1994).
23. S. Samaranyake, A.K. Bajaj, *Nonlinear Dynamics* **4**, 605, (1993).
24. T. Morbiato, R. Vitaliani, A. Saetta, *Computers & Structures* **89**, 1649, (2011).
25. A.P. Willmott, J. Dapena, *Journal of Sports Sciences* **30**, 369, (2012).
26. Y. Suzukia, T. Nomuraa, M. Casadiob, P. Morassoc, *Journal of Theoretical Biology* **310**, 55, (2012).
27. K.P. Granataa, S.E. Wilsonb, *Clinical Biomechanics*, Volume **16**, Issue 8, Pages 650–659 (2001).
28. A. Fradkov, B. Andrievsky, K. Boykov, *Mechatronics* **15**, 1289, (2005).
29. E.J. Doedel, A.R. Champneys, T.F. Fairgrieve, Y.A. Kuznetsov, B. Sandstede, X. Wang
Auto 97: continuation and bifurcation software for ordinary differential equations (1998)